Industrial Chemistry & Materials

ROYAL SOCIETY OF CHEMISTRY

PAPER

View Article Online
View Journal | View Issue

Cite this: *Ind. Chem. Mater.*, 2025, **3**, 363

Effective methane biodegradation through *in situ* coupling with *methanotroph* and HK@SB-1 MOFs†

Weihang Han, [ab] Ruoshi Luo,[b] Dan Wang, *[ab] Tinglan Li,[b] Qin Zhao, [b] Xue Xia,[b] Ge Hu,[b] Zhen Zhou[b] and Yunpei Liang[a]

Methane is a primary greenhouse gas that poses significant risks to the safety of coal mine operations. Microbial methane degradation offers a sustainable and environmentally friendly solution with considerable potential for development. However, the slow mass transfer rate often hinders the process, necessitating improvements to enhance methane degradation efficiency. This research introduces an innovative *in situ* coupling strategy that leverages methanotrophic bacteria's high selectivity and adsorbents' rapid adsorption capabilities. Initially, the dominant strain of methane-degrading bacteria was isolated from rice paddies. Following this, the strain was characterized as *methanotroph* and its physicochemical properties were investigated to optimize its gas-degrading efficiency. Subsequently, the synthesis of HKUST-1@SBA-16 composites was achieved by incorporating mesoporous silica SBA-16 into HKUST-1, resulting in materials with superior stability and adsorption characteristics. Subsequently, accelerated methane biodegradation was achieved through the *in situ* coupling of the *methanotroph* T2 with the HKUST-1@SBA-16 composite. Under optimal conditions, the methane degradation rate within the HKUST-1@SBA-16-T2 system reached 98.65%. This study introduces an innovative approach to the efficacious mitigation of methane emissions achieved by integrating natural microbial processes with metal–organic frameworks (MOFs). This comprehensive strategy is important for preventing coal mine gas outbursts, and this is of great significance and pioneering in the efficient and selective removal of methane using natural bacteria combined with artificial materials.

Received 10th October 2024,
Accepted 16th December 2024

DOI: 10.1039/d4im00131a

rsc.li/icm

Keywords: *Methanotrophs*; MOFs; Methane degradation; Adsorbent; Microbial degradation.

1 Introduction

Coal mine gas is a general term for harmful gases prevalent in coal mines, mainly consisting of methane (CH_4) and small amounts of CO_2, hydrogen sulfide, and other gases.[1] Gas outbursts are a common dynamic disaster in coal mining.[2,3] Methane is a potent greenhouse gas with a global warming potential 20 times greater than CO_2, so the annual increase in methane emissions is a serious global problem.[4] Consequently, Gas reduction is crucial to environmental protection and coal mine production. The traditional methods of gas control in coal mines are gas drainage and drilling drainage.[5] However, due to the increase in coal mining depth, the permeability of coal seams is reduced, leading to the formation of some ultra-low permeability coal seams, the probability of gas explosions remains high, which can lead to serious safety accidents. Therefore, it is necessary to study new methods and technologies to solve coal mine gas problems.

Microbial biocatalysts have an advantage in catalyzing methane processes because they do not require harsh reaction conditions and do not release any toxic byproducts.[6,7] While, selecting appropriate strains is crucial for the catalytic effect among the numerous biocatalysts. *Methanotrophs* are widely present in nature as microorganisms that thrive using methane as their sole carbon source and energy.[8] Studies have shown that *methanotrophs* can effectively degrade methane emissions from biogas, which provides a basis for using microorganisms to treat coal mine gas.[9,10] *Methanotrophs* are widely distributed in soil, swamps, landfills, seafloor, lakes, coal mines, and oil and gas extraction sites.[11–16] *Methanotrophs* were discovered as early as the beginning of the 20th century. Whittenbury R. *et al.* isolated and classified more than 100 species of *methanotrophs* in 1970.[17] Sly *et al.* treated coal mine gas by screening effective strains and constructing a biofilm reactor device. *Methanotrophs* were able to remove a large amount of methane from the

[a] *State Key Laboratory of Coal Mine Disaster Dynamics and Control, Department of Chemical Engineering, Chongqing University, School of Chemistry and Chemical Engineering, 55 Daxuecheng South Road, Shapingba District, Chongqing, 400044, P.R. China. E-mail: dwang@cqu.edu.cn; Tel: +86 23 65678926*
[b] *School of Chemistry and Chemical Engineering, Chongqing University, Chongqing, 400044, P.R. China*

† Electronic supplementary information (ESI) available. See DOI: https://doi.org/10.1039/d4im00131a

methane/air mixture.[18] Although *methanotrophs* can degrade methane under mild conditions, their further applications are limited due to their complex oxidation mechanism and inability to adsorb methane quickly.

At present, many porous adsorption materials with ultra-high specific surface areas have been widely studied because they can quickly adsorb methane gas, such as activated carbon, metal–organic framework materials (MOFs), zeolite, silica gel, carbon molecular sieve, *etc.*[19–22] MOFs materials have high porosity, large specific surface area, and adjustable surface properties. They have more diverse and controllable porous structures than other traditional porous materials. Tate *et al.* found that coating 5A zeolites with MOFs materials such as HKUST-1, Al-MOF, Ga-MOF, and Co-MOF can improve methane adsorption storage performance.[23] Salehi composited the MOFs material MIL-101 with activated carbon and discovered that the composites had higher specific surface area, which led to increased CH_4 storage and capture.[24] Rosado *et al.* utilized a HKUST-1 nanocomposite with graphene oxide to absorb and separate CO_2 and CH_4. The nanostructured HKUST-1@GO composite exhibited high selectivity for CO_2.[25] While adsorbent materials cannot be applied in low-concentration methane environments due to their weak selectivity and adsorption capability for methane. Collecting and utilizing low-concentration gas in coal mines is challenging, and there is a high risk of gas explosion accidents when gas concentrations range between 5% and 16%. Addressing methane emissions is crucial in mitigating the impact of industrial development on the environment and human habitats. It is imperative to explore innovative approaches, such as coupling synthetic MOFs materials with *methanotrophs*, to enhance methane biodegradation and reduce its environmental impact. In addition, coupled cells have higher stability than free cells and are considered adequate to improve bioconversion efficiency.[26–29]

This study developed a coupling strategy that integrates adsorbents' rapid adsorption capabilities with biocatalysis's specificity, enabling the rapid removal of methane from the environment. *Methanotrophs*, which exhibit effective methane oxidation, were isolated from rice paddies. Subsequently, an innovative *in situ* coupling strategy was used to combine MOFs materials with the *methanotrophs*. This cross-disciplinary approach significantly enhances the methane oxidation rate and mitigates the hazards associated with coal mine gas emissions. The strategy facilitates an improved degradation efficiency of methane by *methanotrophs*. The study demonstrates that coupling MOFs materials with biological bacteria can enhance mass transfer between the gas and the strains, thereby improving bioconversion. This approach offers valuable insights for optimizing other bioconversion processes that utilize gas as a raw material.

2 Results and discussion

2.1 Adsorbent morphology characterization

HKUST-1 has a large specific surface area and excellent CH_4 adsorption performance, while its stability is relatively poor. Therefore, HKUST-1 was *in situ* grown on SBA-16 to prepare HK@SB-*n*, which improved the stability and adsorption performance of HKUST-1. Fig. 1 illustrates the microscopic morphology of the adsorbents using SEM. As can be seen from Fig. 1a, HKUST-1 crystals were regular octahedral in shape, with a particle size range of 10–20 μm, smooth surface, and sharp edges and corners. Their structure and morphology were similar to those reported previously.[30,31] As shown in Fig. 1b, it can be seen that SBA-16 exhibits a spherical morphology with distinct particles and a particle size of approximately 4–6 μm. Fig. 1c shows that the morphology of the HK@SB-1 composite material formed by adding SBA-16 to HKUST-1 has changed. The HKUST-1 crystals transformed to octahedral (10–20 μm) to a layered flower-like structure assembled from crystals arranged in layers with a thickness. When SBA-16 was immersed in a copper precursor solution, copper ions quickly aggregated around the silica matrix. Subsequently, these bonded metal centers further connect with the carboxylic acid ligands of terephthalic acid, forming MOF generation sites on the surface of SBA-16. The nanocrystals were generated and connected as the reaction progressed to form nanosheets. These nanosheets continued to grow layer by layer and were orderly arranged on the molecular sieve. In addition, the mesoporous structure of SBA-16 further restricts the excessive expansion of the framework, thus forming the flower-like structure of the composite material. The addition of SBA-16 enhances the thermal stability of HK@SB-1, a feature demonstrated by thermogravimetric characterization (Fig. S3†).

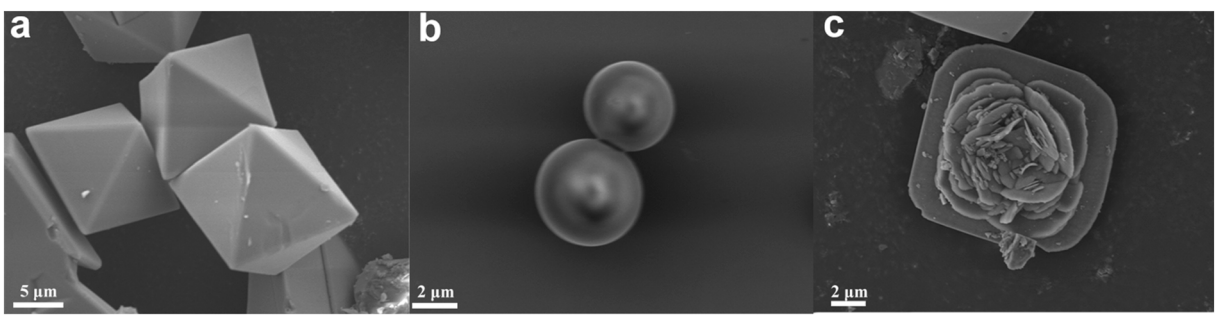

Fig. 1 SEM images of (a) HKUST-1, (b) SBA-16, and (c) HK@SB-1 (1 wt% SBA-16 modified HKUST-1).

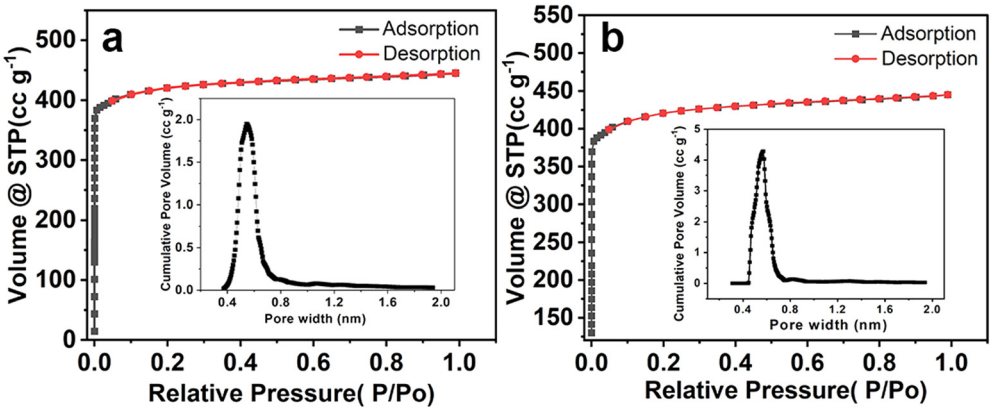

Fig. 2 Isothermal N_2 adsorption and desorption curves of (a) HKUST-1 and (b) HK@SB-1 composites and pore size distribution.

As shown in Fig. 2, The isothermal N_2 adsorption–desorption and pore size distribution curves of HKUST-1 and HK@SB-1 composites were analyzed. These curves exhibit a typical type I isotherm,[32,33] which suggests that the materials primarily consist of a microporous structure. Based on these curves, the surface area of HKUST-1 and HK@SB-1 composites was determined to be 1490.11 $m^2\ g^{-1}$ and 1657.67 $m^2\ g^{-1}$, respectively. The pore size distribution analysis reveals that the primary pore size of both materials was approximately 0.6 nm, indicating a predominance of micropores. Table 1 presents the pore structure parameters of these materials. It can be observed that the addition of SBA-16 initially increases the specific surface area of HKUST-1, but further additions cause a decrease. Among the composites, HK@SB-1 exhibits the largest specific surface area. From the BJH, it can be found that the average pore size of all composites was less than 2 nm, indicating their microporous nature. Micropores enhance a material's surface area, increasing its CH_4 adsorption capacity.[34]

2.2 Adsorbent structure characterization

To analyze the effect of SBA-16 on the crystal structure of HKUST-1, the prepared adsorbent was investigated by XRD and FT-IR. The XRD patterns of the as-synthesized HKUST-1, HK@SB-0.5, HK@SB-1, HK@SB-1.5, and HK@SB-2 were shown in Fig. 3a. The major diffraction peaks of HKUST-1 were observed at 2θ = 6.74°, 9.50°, 11.65°, 13.46°, 19.08°, 25.98°, and 29.31° corresponding to (200), (220), (222), (400), (440), (731), and (751) crystal planes, which coincided with those reported in the literature.[35,36] The diffraction peaks of the HK@SB-*n* series hybrid material were very similar to those of HKUST-1, which indicated that the backbone structure of the original HKUST-1 was maintained in the HK@SB-*n* series materials, and the crystal structure of the MOFs was well preserved. No new peaks of SBA-16 appeared in the composites, which can be attributed to the high dispersion of SBA-16 in the composites and its relatively low content. The crystallinity of HK@SB-*n* decreases with the increase in SBA-16 content.

Table 1 Pore structure parameters of HKUST-1 and HK@SB-*n* composites

Materials	S_{BET} ($m^2\ g^{-1}$)	V_{total} ($cm^3\ g^{-1}$)	Average pore diameter (nm)
SBA-16	498.801	0.2153	1.940
HKUST-1	1490.117	0.6666	1.652
HK@SB-0.5	1598.785	0.6783	1.786
HK@SB-1	1657.675	0.7379	1.781
HK@SB-1.5	1574.274	0.6680	1.795
HK@SB-2	1463.662	0.6566	1.794

The FT-IR spectra of HK@SB-*n* composites were shown in Fig. 3b. The characteristic peaks at 1105 cm^{-1} were attributed to the C–O telescopic vibration peak, while the peak at 732 cm^{-1} could be ascribed to the stretching vibration of Cu–O in HKUST-1. The peaks at 1370 cm^{-1} and 1553 cm^{-1} indicate the presence of asymmetric telescopic vibration peaks of the O–C–O moiety.[37] The peak at 1444 cm^{-1} corresponds to the C=C telescopic vibration peaks in the benzene ring, while the peak at 1649 cm^{-1} corresponds to the C=O telescopic vibration peaks of the carboxylic acid moiety. These characteristic peaks agreed with those reported in the related literature.[35,38] The strong bands observed at 1085 cm^{-1} and 804 cm^{-1} were attributed to the asymmetric stretching of Si–O–Si in the Si–oxygen tetrahedra.[39] The FT-IR spectra of all *in situ* synthesized HK@SB-*n* composites were similar to those of pure HKUST-1. Although the intensity of the two absorption bands associated with Si–O–Si was relatively low, they were still detectable and could serve as evidence for the presence of SBA-16 in the composites.

2.3 Methane adsorption properties of HK@SB-*n* composites

As shown in Fig. 4, CH_4 isothermal adsorption tests were performed on SBA-16, HKUST-1, and composite HK@SB-*n* at 330 K under atmospheric conditions. The composite material HK@SB-*n* exhibits CH_4 adsorption capacity that initially increases and then decreases with the increase of SBA-16 content. Among them, the composite material HK@SB-1 exhibits the highest CH_4 adsorption capacity due to its larger

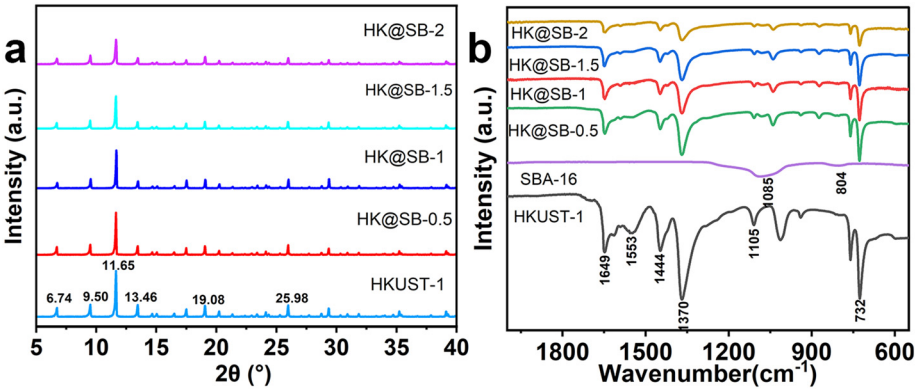

Fig. 3 (a) XRD analysis of the crystal structure of HKUST-1 and HK@SB-*n*; (b) FT-IR spectrum analysis of the crystal composition of HKUST-1 and HK@SB-*n*.

micropore volume and specific surface area compared to other materials. The CH_4 adsorption capacity of all composite materials was higher than that of SBA-16. This was because a small amount of SBA-16 was added, which forms a nano-flower structure by affecting the growth of HKUST-1. On the one hand, the nano-flower structure leads to an increase in total pore volume, which allows gas to flow faster. It also increases the specific surface area of the material, providing more area for the material to come into contact with CH_4. The increase in micropore volume was more conducive to CH_4 adsorption. When an excessive amount of SBA-16 was added, the specific surface area of HK@SB decreased, which had an adverse effect on the CH_4 adsorption performance.

2.4 Molecular identification of *methanotrophs* bacteria

The DNA of *methanotrophs* from rice field was extracted using TSINGKE plant DNA extraction kit, and amplification of 16S rDNA gene were performed using universal bacterial primer pairs 27F (5′-AGTTTGATCMTGGCTCAG-3′) and 1492R (5′-CGGYTACCTTGTTACGAC-3′). Subsequently, the amplified product was subjected to gel electrophoresis, and the electrophoresis diagram is depicted in Fig. S1.† It can be observed from the electrophoresis diagram that the PCR amplified electrophoresis strip was relatively straightforward and consistent, the left and right symmetry of the band has no signal interference, the position of the reaction band is around 1500 bp, and after sequencing the PCR product, a total of 1399 bp. The PCR product was sequenced to obtain the specific sequence: >*methanotrophs bacteria*-Contig1 (specific sequence refer to the ESI†).

The 16S rDNA sequence obtained from methanotrophic bacteria T2 was uploaded to the NCBI database website, and then the sequences were compared. Sequences were selected and a phylogenetic tree was constructed using MAGE 7.0 software. The construction method was the maximum likelihood method. The phylogenetic tree of *methanophiles* is depicted in Fig. S2.† The numbers displayed at the tree nodes represent the confidence level of the evolutionary relationship between different species branches. A confidence level exceeding 66 is considered credible. Fig. S2† shows that strain *methanophiles* was closely related to the genus *Methylophilus methylotrophus* (KF911346.1 *methylophilus methylotrophus*). The confidence level for this relationship is 97, indicating a high level of certainty.

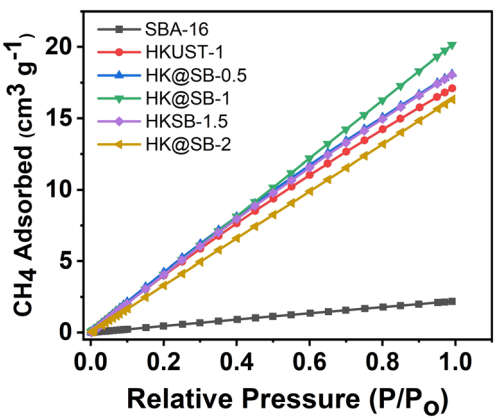

Fig. 4 Comparative analysis of the adsorption performance of HKUST-1, SBA-16 and modified HK@SB-*n*.

2.5 Activity of *methanotrophs* bacteria

Optimization of bioprocess parameters, such as pH and temperature, is crucial for the growth of methanotrophic bacteria. Fig. 5 shows the degradation of CH_4 by *methanotrophs* and their growth under different conditions. The effect of temperature on the growth of *methanophiles* can be found in Fig. 5a, it was found that the OD_{600} value gradually increased with the increase in temperature, peaking at 30 °C. While beyond 30 °C, the OD_{600} value gradually decreased, which indicates that the optimal growth temperature for the *methanophiles* is 30 °C, with an optimal growth temperature range of 30–35 °C. As shown in Fig. 5b, with the increase in pH, the OD_{600} values gradually increased. The highest OD_{600} value was observed at pH = 7.0. However, beyond pH = 7.0, the OD_{600} values gradually decreased. It is indicates that the optimal growth pH for the

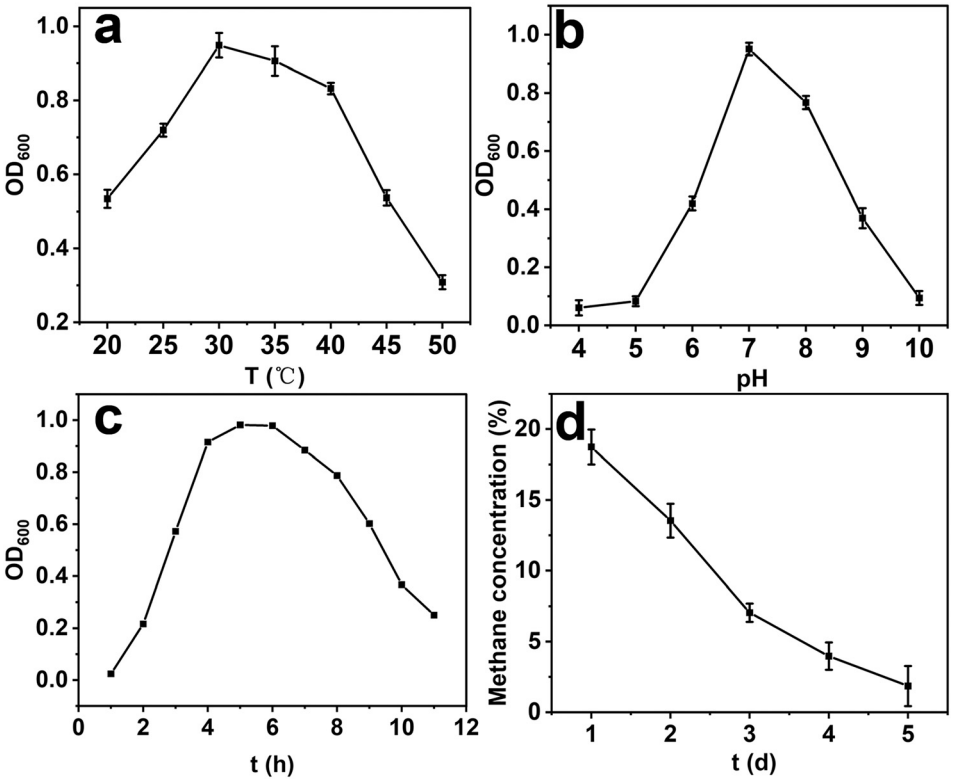

Fig. 5 (a) Effect of temperature, and (b) pH on the growth of *methanotroph*; (c) the growth curve of the *methanotrophs* under optimal conditions; (d) changes in methane content during the growth of *methanotroph*.

strain is 7.0. The growth pattern of the *methanophiles* under optimal conditions can be observed in Fig. 5c. On the third day, the bacterium entered the logarithmic growth phase. From the fourth to the sixth day, it reached a plateau phase where the growth rate remained relatively constant. After six days, the growth of the bacterium declined, resulting in a decrease in cell viability. The growth cycle of the bacterium was found to be around 10–11 days, with the highest growth observed on the sixth day. The change in CH_4 content in the bottle during the growth process was monitored using a gas chromatograph and shown in Fig. 5d, it was found that the concentration of CH_4 continuously decreased during the cultivation period of the *methanotrophs*. By the fifth day of cultivation, the CH_4 concentration declined from the initial 20% to 2.11%, resulting in a CH_4 degradation efficiency of 89.45%. The fastest CH_4 degradation rate was observed on the second to third day. It can be concluded that this strain has a good ability to oxidize CH_4.

2.6 *In situ* coupling of *methanotrophs* with HKUST-1@SBA-16

Methanotrophs T2 was *in situ* coupled with HKUST-1@SBA-16 composite material to prepare HK@SB-T2. As displayed in Fig. 6, the SEM images confirmed the growth of the *methanotrophs* T2 on the synthesized flower-shaped composite material HKUST-1@SBA-16. Compared to free *methanotrophs* T2, the bacterial cells were embedded on the surface of the material. The petal structure of the composite

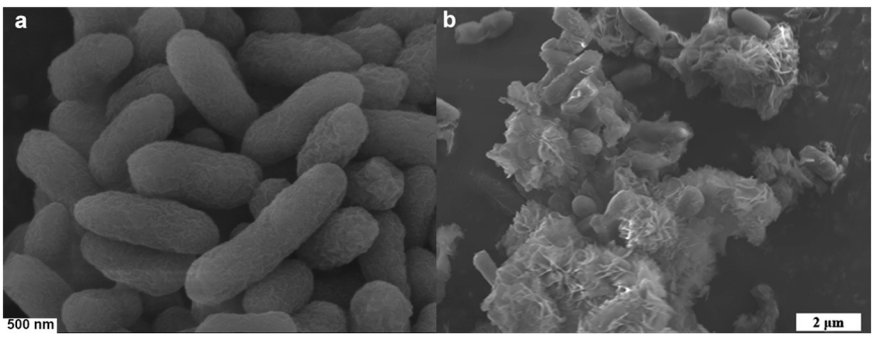

Fig. 6 SEM images of (a) free cells (control strain) and (b) HK@SB-T2 (coupling strains).

material provides more loading sites for the bacteria, reducing microbial aggregation and increasing the contact area between the bacteria and methane.

It can be found that *methanotrophs* T2 was embedded in the surface of the material from SEM. In order to analyze the effect of *methanotrophs* T2 on the adsorption performance of the HK@SB-1, the isothermal N_2 adsorption–desorption curve of HK@SB-T2 was analyzed using BET shown in Fig. 7a. According to these curves, the surface area of the HK@SB-T2 composite material was determined to be 870.11 m^2 g^{-1}, which is significantly reduced relative to the specific surface area of HK@SB-1. In addition, the adsorption of CH_4 by HK@SB-T2 was analyzed. From Fig. 7b, the CH_4 isothermal adsorption tests by HK@SB-T2 are lower than that of HK@SB-1. This is because *methanotrophs* T2 is embedded in the surface of the material, which reduces the specific surface area of HK@SB-1, further affecting the adsorption performance of HK@SB-T2 for CH_4.

As shown in Fig. 8a, the CH_4 degradation reaction was performed using different dosages of HK@SB-1 composites coupled with *methanotrophs* T2. It was demonstrated that the CH_4 degradation rate increases as the dosage of HK@SB-1 composites increases. Additionally, the overall CH_4 degradation efficiency of the coupled cell system surpasses that of the free cells. However, a significant decrease in the CH_4 degradation rate occurs when the amount of coupled carriers reaches 20 mg and 25 mg. This decline was attributed to the excessive encapsulation of *methanotrophs* T2 caused by a large amount of carriers. Consequently, the CH_4 gas fails to adequately interact with the bacterial strains, resulting in increased mass transfer resistance. The overall degradation efficiency of CH_4 reached 98.65% when the coupled carrier was added at 15 mg.

Glutaraldehyde (GA) is a commonly used cross-linking and fixing agent. The solution contained two aldehyde groups that could undergo non-specific condensation reactions with amino groups, thereby facilitating structural fixation.[40–42] Fig. 8b illustrates the CH_4 degradation curve by HK@SB-T2 in various concentrations of GA immobilization systems. The CH_4 degradation efficiency of the coupled cell system initially increases and then decreases with increasing concentrations of GA. At concentrations of 10, 30, and 50 mM, the CH_4 degradation rate of the coupled cell system increases with higher GA concentration. The highest CH_4 degradation rate was observed at a GA concentration of 50 mM. It was possible that the cross-linking between GA and amino groups on the cell membrane enhances the activity of the coupled cells. Additionally, with GA concentrations of 70 mM and 90 mM, the CH_4 degradation rate decreases as the concentration increases. This was attributed to the inherent toxicity of GA, as high concentrations can negatively impact cell activity.[43]

Biological activity was readily affected by pH, which influences cell membrane proteins and extracellular hydrolase activity.[44–46] A broad range of buffer solutions were prepared with pH values of 4.0, 5.0, 6.0, 7.0, and 8.0 to investigate the effect of pH on the activity of coupled cell systems in CH_4 degradation. As shown in Fig. 8c, the CH_4 degradation rate initially increases and then decreases at different pH levels. When the pH = 4, the CH_4 degradation rate was prolonged, this is because the activity of *methanotrophs* T2 decreases sharply in an acidic environment and cannot continuously consume CH_4 in the environment. Moreover, *methanotrophs* T2 growth is inhibited in an environment with pH = 5. However, HK@SB-T2 shows a better ability to CH_4 degradation when the *in situ* coupling of the *methanotroph* T2 with the HKUST-1@SBA-16 composite. This suggests that *methanotrophs* T2 ability to adapt to different environmental circumstances is improved when the *in situ* coupling of the *methanotroph* T2 with HK@SB-1. In addition, the CH_4 degradation rate gradually increases as the pH rises. The coupled-cell system demonstrates good overall performance in CH_4 degradation at pH levels of 6 to 8. The optimal coupling condition occurs at pH = 7, and the CH_4 removal rate of the coupled cell system starts to decrease.

As shown in Fig. 8d, temperature significantly impacts the degradation rate of the coupled cell system. With increasing temperature, the rate of CH_4 degradation initially increases and then decreases. The maximum CH_4 degradation rate was observed at 30 °C. Temperatures higher or lower than 30 °C

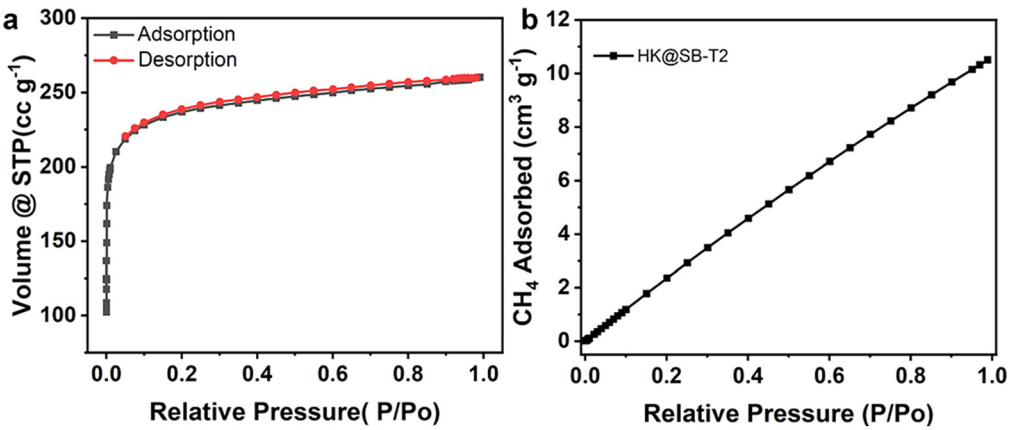

Fig. 7 (a) Isothermal N_2 adsorption and desorption curves and (b) CH_4 adsorption performance of HK@SB-T2.

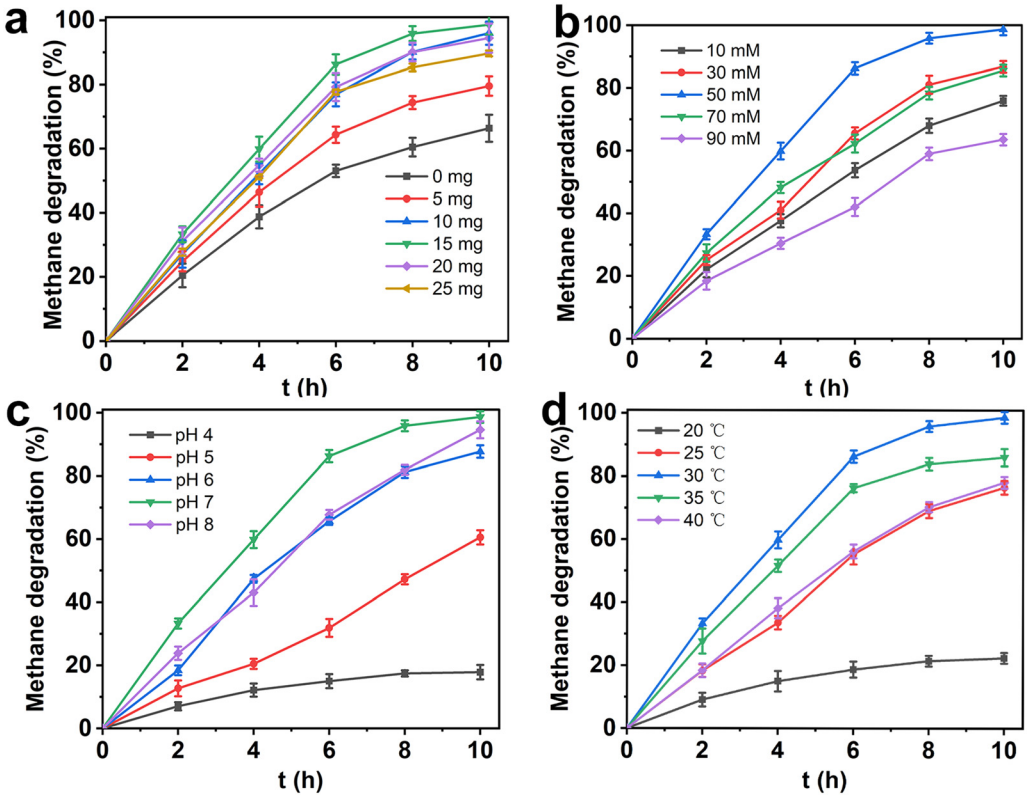

Fig. 8 (a) Effect of different masses of HK@SB-1 on methane degradation (50 mM glutaraldehyde, pH = 7, 30 °C); (b) effect of different concentrations of glutaraldehyde on methane degradation (15 mg HK@SB-1, pH = 7, 30 °C); (c) effect of different pH on methane degradation (15 mg HK@SB-1, 50 mM glutaraldehyde, 30 °C); (d) effect of different temperatures on methane degradation (15 mg HK@SB-1, 50 mM glutaraldehyde, pH = 7). Error bars indicate the standard deviations of three independent experiments.

can affect the activity of enzymes, with high temperatures potentially leading to enzyme inactivation.

Coupling HK@SB-1 with *methanotrophs* enhances the *methanotroph's* capacity to adapt to different environments. *Methanotrophs* absorb CH_4 as their sole source of carbon and energy, and HK@SB-1 adsorbs and enriches CH_4 for *methanotrophs*, providing a conducive growth environment. In a methane environment, HK@SB-T2 first enriches CH_4 through HK@SB-1. *Methanotrophs* use intracellular enzymes including methane monooxygenase (MMO), methanol dehydrogenase (MDH), formaldehyde dehydrogenase (FADH), and formate dehydrogenase (FDH) sequential catalysis. First, CH_4 was oxidized to methanol by MMO. MMO can activate the strong C–H bonds in methane at standard temperature and pressure, and oxygen can oxidize it to methanol. After the first step of CH_4 conversion, methanol was oxidized to formaldehyde by MDH. Formaldehyde can be further oxidized or assimilated. Formaldehyde was first converted to

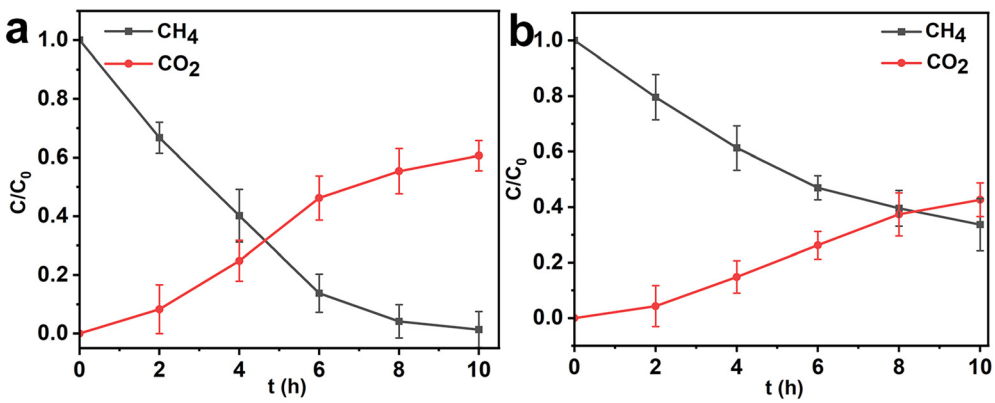

Fig. 9 Changes in CH_4 and CO_2 in the (a) HK@SB-T2 and (b) free cell methane degradation system (gas composition in the reactor was analyzed using gas chromatography every 2 hours). Error bars indicate the standard deviations of three independent experiments.

formic acid by formaldehyde dehydrogenase (FADH). Finally, formic acid dehydrogenase (FDH) oxidizes formic acid to CO_2.[47] The reaction process detects the gas in the shake flask. As shown in Fig. 9a, the methane gas in the shake flask gradually degraded, and the final degradation rate reached 98.65%. However, the CO_2 generation rate was only 60.6%, which was attributed to the increase in CO_2 concentration inhibiting the further conversion of methanol.[48] In addition, the CH_4 degradation process of free *methanotroph* cells is shown in Fig. 9b. In this process, 67.4% of CH_4 can be degraded and 42.6% of CO_2 can be produced, which demonstrates that the process from CH_4 to CO_2 requires the participation of multiple enzymes. After eight hours, the CO_2 generation efficiency reduced when the concentration reached 37.3%. This finding showed that HK@SB-T2 can increase CH_4 degradation capacity. Furthermore, high CO_2 concentration in the environment will affect the degradation and conversion of CH_4 by methanotrophic bacteria.[49,50]

2.7 Stability and recyclability of HK@SB-T2

To demonstrate the stability and recyclability of HK@SB-T2, repeated batch CH_4 degradation was evaluated for five cycles of reuse. As shown in Fig. 10. The composite still showed an 86% degradation capability after the fifth cycle, although the CH_4 degradation efficiency had decreased from the initial use. It is suggested that HKUST-1@SBA-16-T2 has good stability and recyclability for CH_4 degradation.

3 Conclusions

This study introduces an innovative *in situ* coupling strategy that leverages methanotrophic bacteria's high selectivity and adsorbents' rapid adsorption capabilities. *Methanotrophs* T2, screened from rice paddies, can decompose low-concentration CH_4. The HK@SB-1 composite material modified based on HKUST-1 exhibits good biocompatibility and a large specific surface area. Then, *methanotrophs* T2 was *in situ* coupled to HK@SB-1 in phosphate buffer solution through adsorption and covalent bonding methods. In this process, the HK@SB-1 composite provided active sites for material *methanotrophs* T2, enabling simultaneous CH_4 adsorption and degradation, thus facilitating an effective CH_4 adsorption degradation. The results showed that the optimal conditions for the adsorption-microbial degradation *in situ* coupled process were 15 mg HK@SB-1 composite material, 30 mM glutaraldehyde, pH = 7, and a reaction temperature of 30 °C. Under these conditions, after reacting for 10 hours, the CH_4 degradation rate reached 98.65%. Compared with the degradation efficiency of a single strain, the degradation efficiency increased by 1.6 times, effectively improving the degradation efficiency of *methanotrophs* T2. The coupled material adsorption-microbial degradation systems provide new insights into low-cost and efficient CH_4 degradation. This innovative method effectively removes low-concentration gas in coal mines and paves the way for research on effectively preventing coal mine gas explosions.

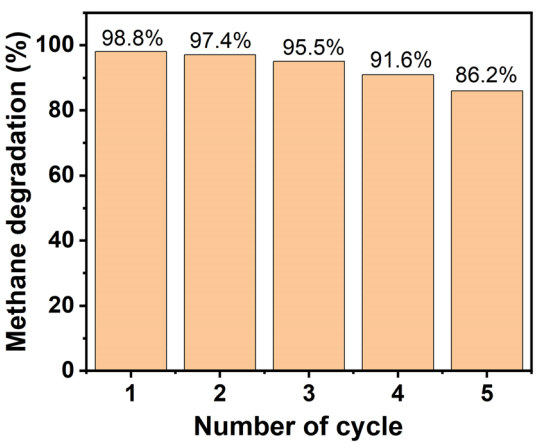

Fig. 10 The stability and recyclability of HK@SB-T2.

4 Experimental section

4.1 Materials

Glutaraldehyde (GA), *n*-butanol was purchased from Chengdu Cologne Chemicals Co., Ltd, hydrochloric acid was purchased from Chongqing Chuandong Chemical (Group) Co., Ltd, copper nitrate trihydrate ($Cu(NO_3)_2{\cdot}3H_2O$) was purchased from Guangdong Guanghua Science and Technology Co., Ltd, Pluronic F127 copolymer was purchased from Sinopharm Chemical ReagentCo., Ltd; tetraethoxysilane was purchased from Shanghai Bide Pharmaceuticals Co., Ltd, trimesic acid (H_3BTC) from Shanghai Bide Pharmaceuticals Co., Ltd, methane from Chongqing Jiaqing Gas Co., Ltd.

4.2 Procedures of synthesis

HKUST-1. HKUST-1 was prepared by the solvent method. 1.087 g $Cu(NO_3)_2{\cdot}3H_2O$ was dissolved in 15 mL deionized water and stirred until completely dissolved to form solution A. 0.525 g H_3BTC was dissolved in 15 mL of anhydrous ethanol and stirred until completely dissolved to form solution B. Solution A was added to solution B and transferred the mixture to a 100 mL reaction vessel lined with polytetrafluoroethylene (PTFE), then the reaction was carried out in an oven at a constant temperature of 120 °C for 12 h. After the reaction, the mixture was cooled down naturally to room temperature. The blue solid was centrifuged and washed with deionized water and ethanol thrice each. Subsequently, the solid sample was finally dried under vacuum at 70 °C for 24 h to obtain HKUST-1.

SBA-16. 1 g Pluronic F127 copolymer was dissolved in 48 mL distilled water. Then, 2 ml concentrated hydrochloric acid (HCl, 37 wt%) was added to the solution. After stirring for 30 minutes, 3 ml butanol was added to the solution as a co-surfactant. The mixture was stirred for 1 hour, and then 4.73 g tetraethoxysilane was added to the solution. The mixture was kept at 40 °C for 24 hours, and then the solution container was subjected to a hydrothermal process at 80 °C for 48 hours. Afterward, the mixture was filtered

and washed six times with distilled water. The white powder obtained was dried at 100 °C for 12 hours. Subsequently, it was calcined at 550 °C for 5 hours to eliminate the Pluronic F127 copolymer template.

HKUST-1@SBA-16. The hybrid material based on HKUST-1 and SBA-16 was prepared using an *in situ* solvothermal method. In summary, 1.050 g H_3BTC was dissolved in 30 mL of ethanol to form a transparent solution. Meanwhile, a certain amount of SBA-16 was dispersed in a solution of copper nitrate (2.174 g $Cu(NO_3)_2{\cdot}3H_2O$ mixed with 30 mL of deionized water) and sonicated for 30 minutes. The two solutions were combined in a PTFE-sealed reactor and stirred for 30 minutes. The mixture was heated to 120 °C and maintained at this temperature for 12 hours. After cooling to room temperature, the solid product was centrifuged and washed several times with ethanol. The sample was dried at 70 °C to obtain the hybrid material, referred to as HK@SB. Depending on the different amounts of SBA-16 added, the resulting composite materials were labeled as HK@SB-*n* (*n* = 0.5, 1, 1.5, 2).

4.3 Cultivation of *methanotrophs*

10 g soil was collected from a wet paddy field (Dianjiang, Chongqing), added to 30 ml sterilized deionized water, shaken well, sealed, and left to stand. 10 mL of the standing supernatant was added to a 100 mL sterilized inorganic salt (NMS) medium and 10% methane was used as the carbon source. The mixture was sealed and enriched in a constant temperature shaker at 30 °C and 180 r min^{-1}. The first cultural cycle was 7 days. Afterward, 5 mL of the bacterial suspension from each sample was taken and transferred to a new medium under the same culture conditions for 4–5 days. This culture process was repeated at a later stage. The generation and identification can then be carried out.

The *methanotrophs* were inoculated into NMS medium respectively, and the growth of *methanotrophs* was observed with CH_4 as carbon source. The OD_{600} of the strains was measured at different temperatures (20–50 °C) and pH (pH = 4–10) for 96 hours to analyze the optimal growth conditions for methanotrophic bacteria, the reaction pH was adjusted using sodium acetate (pH = 4–5) and phosphate (pH = 6–8).

4.4 Generation and identification of *methanotrophs*

1 mL of bacterial liquid was drawn from the mixed bacterial culture solution, centrifuged, and then the supernatant was discarded. The liquid was inoculated on a solid culture medium with an inoculation loop, and CH_4 was used as the carbon source. The culture was grown in a constant temperature incubator at 30 °C for 4–5 days. After a single colony grows on the plate, a single colony is picked with a machine ring, and the plate streaking method is used for inoculation and culture. The above steps are repeated. After multiple streaking cultures, a pure strain of *methanotrophs* is obtained. At this time, the morphology of the single colony of *methanotrophs* on the plate can be observed. *Methanotrophs* on the plate can be observed. Pick a single colony and put it into NMS liquid culture medium for enrichment culture to obtain a pure bacterial liquid.

The plate spreading method spreads the *methanotrophs* enriched by liquid culture on the solid culture medium. Methane was injected into the culture dish and sealed with plastic wrap. The dish was then inverted and placed in a constant temperature incubator for culture at 30 °C until a single colony developed. After three generations, single colonies with good growth density were selected and cultured in a sterilized NMS liquid medium with 10% CH_4 as the carbon source. The cultures were placed on a shaker at 30 °C and 180 rpm until the medium became turbid. During this period, the CH_4 content in the culture medium was measured every 1–2 days. The strains were sequenced using 16S rDNA. The screened *methanotrophs* were named T2.

4.5 Preparation of complex HK@SB-T2

Methanotrophs T2 was *in situ* coupled with HKUST-1@SBA-16 to obtain a composite material. Under 100 rpm shaking, 50 mg stem cells were added to 10 mL phosphate buffer (pH = 7.0). Then HKUST-1@SBA-16 was added as a coupled carrier and shaken for 10 min. Then, an appropriate amount of GA was added and shaken to allow adsorption for 1 h, washed once with distilled water to remove excess GA solution, and washed with a buffer solution to eliminate loosely attached cells. This process resulted in a fixed cell system named HK@SB-T2, which was stored at 4 °C for future use.

4.6 Degrading methane of HK@SB-T2

When the gas concentration is between 5% and 16%, it is easy to cause explosion accidents. In order to better analyze the gas degradation process of HK@SB-T2, the 20% concentration of methane gas was selected to simulate the gas found in coal mines. First, the HK@SB-T2 were inoculated into 100 mL of NMS medium, 20% methane gas was injected as a carbon source for sealed culture at 30 °C and 180 RPM min^{-1}, the CH_4 concentration was monitored every two hours.

4.7 Effect of HK@SB-T2 on methane degradation

When preparing HK@SB-T2, different contents of HK@SB-1 composite materials (0, 5, 10, 15, 20, 25 mg) were added to analyze the effect of HK@SB content on methane degradation. The concentration of glutaraldehyde (0, 10, 30, 50, 70, 90 mM) was changed to analyze the effect of glutaraldehyde concentration on methane degradation. In addition, sodium acetate (pH = 4–5) and phosphate (pH = 6–8) buffer solutions were used to adjust the reaction pH during the degradation of methane by HK@SB-T2 to analyze the effects of different pH on methane degradation. The reaction temperature was adjusted to 20, 25, 30, 35, and 40 °C to analyze the effect of temperature on methane degradation. During the experiment, the shaking speed was

controlled at 180 RPM min^{-1}, and the methane concentration was measured every 2 h.

4.8 Methane degradation under repeated batch conditions

Repeated methane degradation by HK@SB-T2 was assessed using 20% CH_4 simulated coal mine gas for five cycles of reuse. After each cycle, HK@SB-T2 was collected by centrifugation and further washed with buffer to serve as inoculum for subsequent cycles.

4.9 Characterization of HK@SB-T2

The fixed cells were washed twice with pH 7.0, 100 mM PBS buffer, and then immersed in 2.5% (v/v) glutaraldehyde electron microscopy fixative overnight in a refrigerator at 4 °C to preserve the sample. Then, the sample was washed twice with 100 mM PBS buffer to remove the glutaraldehyde fixative. It was then dehydrated stepwise using 30%, 50%, 70%, 80%, 90%, and 95% ethanol, with each concentration applied for 15 minutes. Subsequently, the sample was dehydrated with anhydrous ethanol twice for 20 minutes each time and allowed to air dry to a constant weight. Finally, the sample was subjected to BET and SEM characterization.

4.10 Analysis methods

Optical density (OD_{600}) measurements were performed using a TU-1901 spectrophotometer at a wavelength of 600 nm to ascertain the absorbance of the bacterial liquid and to monitor the growth kinetics of the T2 strain. Methane was determined by GC9800 gas chromatograph, the column was American Agilent WAX capillary column (30 m column), the detector was hydrogen flame detector (FID). The XRD patterns of samples were recorded using a PANalytical X'Pert Powder from Malvern, the Netherlands. A scanning electron microscope (SEM, Zeiss Sigma 500) was used to detect the morphology of samples. The adsorption–desorption isotherms for N_2 were measured on a max-II unit manufactured by Macchik Bayer in Japan. The CH_4 adsorption performance of the materials was tested on a high-performance fully automated gas adsorption analyzer, Kantar Autosorb-IQ-MP (USA). The samples were tested by thermogravimetric analysis to characterize their thermal stability using a TGA2 thermogravimetric analyzer manufactured by METTLER TOLEDO, Switzerland.

Data availability

Data is available on request from the authors. The data that support the findings of this study are available from the corresponding author.

Conflicts of interest

We declare that we do not have any commercial or associative interest that represents a conflict of interest in connection with the work submitted.

Acknowledgements

This work was supported by the National Key Research and Development Program of China (2022YFC2105700), Scientific Research Foundation of State Key Lab of Coal Mine Disaster Dynamics and Control (2011DA105287-ZR202002 and 2011DA105287-FW202103), the Chongqing Outstanding Youth Fund (cstc2021jcyj-jqX0013), Human Resources and Social Security Bureau of Chongqing (cx2023036), and the National Natural Science Foundation of China (22378032).

References

1 A. K. Singh and J. N. Sahu, Coal mine gas: A new fuel utilization technique for India, *Int. J. Green Energy*, 2018, **15**, 732–743.
2 X. Chen, L. Li, L. Wang and L. Qi, The current situation and prevention and control countermeasures for typical dynamic disasters in kilometer-deep mines in China, *Saf. Sci.*, 2019, **115**, 229–236.
3 K. Wang and F. Du, Coal-gas compound dynamic disasters in China: A review, *Process Saf. Environ. Prot.*, 2020, **133**, 1–17.
4 S. K. S. Patel, M. S. Jeon, R. K. Gupta, Y. Jeon, V. C. Kalia, S. C. Kim, B. K. Cho, D. R. Kim and J.-K. Lee, Hierarchical macroporous particles for efficient whole-cell immobilization: Application in bioconversion of greenhouse gases to methanol, *ACS Appl. Mater. Interfaces*, 2019, **11**, 18968–18977.
5 W. Yang, B. Lin, Y. Gao, Y. Lv, Y. Wang, X. Mao, N. Wang, D. Wang and Y. Wang, Optimal coal discharge of hydraulic cutting inside coal seams for stimulating gas production: A case study in Pingmei coalfield, *J. Nat. Gas Sci. Eng.*, 2016, **28**, 379–388.
6 C.-C. Wang, C.-H. Li and C.-F. Yang, Acclimated methanotrophic consortia for aerobic co-metabolism of trichloroethene with methane, *Int. Biodeterior. Biodegrad.*, 2019, **142**, 52–57.
7 K. K. Sahoo, G. Goswami and D. Das, Biotransformation of methane and carbon dioxide into high-value products by methanotrophs: Current state of art and future prospects, *Front. Microbiol.*, 2021, **12**, 636486.
8 H. Jiang, Y. Chen, P. Jiang, C. Zhang, T. J. Smith, J. C. Murrell and X.-H. Xing, Methanotrophs: Multifunctional bacteria with promising applications in environmental bioengineering, *Biochem. Eng. J.*, 2010, **49**, 277–288.
9 L. C. Jeffrey, D. T. Maher, E. Chiri, P. M. Leung, P. A. Nauer, S. K. Arndt, D. R. Tait, C. Greening and S. G. Johnston, Bark-dwelling methanotrophic bacteria decrease methane emissions from trees, *Nat. Commun.*, 2021, **12**, 2127.
10 Y.-M. Wu, J. Yang, X.-L. Fan, S.-F. Fu, M.-T. Sun and R.-B. Guo, Corrigendum to "Elimination of methane in exhaust gas from biogas upgrading process by immobilized methane-oxidizing bacteria", *Bioresour. Technol.*, 2018, **260**, 432.
11 Y. Fu, Y. Li and M. Lidstrom, The oxidative TCA cycle operates during methanotrophic growth of the Type I

methanotroph Methylomicrobium buryatense 5GB1, *Metab. Eng.*, 2017, **42**, 43–51.

12 W. Zhang, X. Ge, Y.-F. Li, Z. Yu and Y. Li, Isolation of a methanotroph from a hydrogen sulfide-rich anaerobic digester for methanol production from biogas, *Process Biochem.*, 2016, **51**, 838–844.

13 D. H. Hur, J.-G. Na and E. Y. Lee, Highly efficient bioconversion of methane to methanol using a novel type I Methylomonas sp. DH-1 newly isolated from brewery waste sludge, *J. Chem. Technol. Biotechnol.*, 2017, **92**, 311–318.

14 M. S. Samad and S. Bertilsson, Seasonal variation in abundance and diversity of bacterial methanotrophs in five temperate lakes, *Front. Microbiol.*, 2017, **8**, 142.

15 J. P. Sheets, X. Ge, Y.-F. Li, Z. Yu and Y. Li, Biological conversion of biogas to methanol using methanotrophs isolated from solid-state anaerobic digestate, *Bioresour. Technol.*, 2016, **201**, 50–57.

16 H. J. M. Op den Camp, T. Islam, M. B. Stott, H. R. Harhangi, A. Hynes, S. Schouten, M. S. M. Jetten, N.-K. Birkeland, A. Pol and P. F. Dunfield, Environmental, genomic and taxonomic perspectives on methanotrophic Verrucomicrobia, *Environ. Microbiol. Rep.*, 2009, **1**, 293–306.

17 R. Whittenbury, K. C. Phillips and J. F. Wilkinson, Enrichment, isolation and some properties of methane-utilizing bacteria, *J. Gen. Microbiol.*, 1970, **61**, 205–218.

18 L. I. Sly, L. J. Bryant, J. M. Cox and J. M. Anderson, Development of a biofilter for the removal of methane from coal mine ventilation atmospheres, *Appl. Microbiol. Biotechnol.*, 1993, **39**, 400–404.

19 D. Ursueguía, E. Díaz and S. Ordóñez, Metal-organic frameworks (MOFs) as methane adsorbents: From storage to diluted coal mining streams concentration, *Sci. Total Environ.*, 2021, **790**, 148211.

20 T. A. Makal, J.-R. Li, W. Lu and H.-C. Zhou, Methane storage in advanced porous materials, *Chem. Soc. Rev.*, 2012, **41**, 7761–7779.

21 B. Li, H.-M. Wen, W. Zhou, J. Q. Xu and B. Chen, Porous metal-organic frameworks: Promising materials for methane storage, *Chem*, 2016, **1**, 557–580.

22 H. Li, L. Li, R.-B. Lin, W. Zhou, Z. Zhang, S. Xiang and B. Chen, Porous metal-organic frameworks for gas storage and separation: Status and challenges, *Energy Chem.*, 2019, **1**, 100006.

23 K. L. Tate, S. G. Li, M. Yu and M. A. Carreon, Zeolite adsorbent-MOF layered nanovalves for CH_4 storage, *Adsorption*, 2017, **23**, 19–24.

24 S. Salehi and M. Hosseinifard, Evaluation of CO_2 and CH_4 adsorption using a novel amine modified MIL-101-derived nanoporous carbon/polysaccharides nanocomposites: Isotherms and thermodynamics, *Chem. Eng. J.*, 2021, **410**, 128315.

25 A. Rosado, A. Borras, J. Fraile, J. A. R. Navarro, F. Suarez-Garcia, K. C. Stylianou, A. M. Lopez-Periago, J. Giner Planas, C. Domingo and A. Yazdi, HKUST-1 metal-organic framework nanoparticle/graphene oxide nanocomposite aerogels for CO_2 and CH_4 adsorption and separation, *ACS Appl. Nano Mater.*, 2021, **4**, 12712–12725.

26 S. K. S. Patel, V. Kumar, P. Mardina, J. Li, R. Lestari, V. C. Kalia and J.-K. Lee, Methanol production from simulated biogas mixtures by co-immobilized Methylomonas methanica and Methylocella tundrae, *Bioresour. Technol.*, 2018, **263**, 25–32.

27 M.-Y. Zhuang, C. Wang, M.-Q. Xu, X.-M. Ling, J.-J. Shen and Y.-W. Zhang, Using concanavalinA as a spacer for immobilization of E. coli onto magnetic nanoparticles, *Int. J. Biol. Macromol.*, 2017, **104**, 63–69.

28 M.-T. Sun, Z.-M. Yang, S.-F. Fu, X.-L. Fan and R.-B. Guo, Improved methane removal in exhaust gas from biogas upgrading process using immobilized methane-oxidizing bacteria, *Bioresour. Technol.*, 2018, **256**, 201–207.

29 M.-X. Wang, Q.-L. Zhang and S.-J. Yao, A novel biosorbent formed of marine-derived Penicillium janthinellum mycelial pellets for removing dyes from dye-containing wastewater, *Chem. Eng. J.*, 2015, **259**, 837–844.

30 T. Zhao, M. Zou, P. Xiao, M. Luo and S. Nie, Template-free synthesis and multifunctional application of foam HKUST-1, *Inorg. Chem.*, 2023, **62**, 14659–14667.

31 Z. Chen, X. He, J. Ge, G. Fan, L. Zhang, A. M. Parvez and G. Wang, Controllable fabrication of nanofibrillated cellulose supported HKUST-1 hierarchically porous membranes for highly efficient removal of formaldehyde in air, *Ind. Crops Prod.*, 2022, **186**, 115269.

32 J. Guan, Y. Fang, T. Zhang, L. Wang, H. Zhu, M. Du and M. Zhang, Kelp-derived activated porous carbon for the detection of heavy metal ions via square wave anodic stripping voltammetry, *Electrocatalysis*, 2020, **11**, 59–67.

33 Z. Ma, C. Liu, C. Srinivasakannan, L. Li and Y. Wang, Synthesis of magnetic Fe_3O_4-HKUST-1 nanocomposites for azo dye adsorption, *Arabian J. Chem.*, 2023, **16**, 104767.

34 R. Liu, J. Wang, J. Zhang, S. Xie, X. Wang and Z. Ji, Honeycomb-like micro-mesoporous structure TiO_2/sepiolite composite for combined chemisorption and photocatalytic elimination of formaldehyde, *Microporous Mesoporous Mater.*, 2017, **248**, 234–245.

35 C. Chen, Z. Wu, Y. Que, B. Li, Q. Guo, Z. Li, L. Wang, H. Wan and G. Guan, Immobilization of a thiol-functionalized ionic liquid onto HKUST-1 through thiol compounds as the chemical bridge, *RSC Adv.*, 2016, **6**, 54119–54128.

36 P. Jagódka, K. Matus and A. Łamacz, On the HKUST-1/GO and HKUST-1/rGO composites: The impact of synthesis method on physicochemical properties, *Molecules*, 2022, **27**, 7082.

37 P. Sharma, A. Jatrana, S. Mondal, S. Maan and V. Kumar, A promising HKUST-1@SiO_2 composite for the effective adsorption of chlorpyriphos from aqueous medium, *ChemistrySelect*, 2023, **8**, e202204312.

38 Z. Zhang, W. Huang, X. Li, X. Wang, Y. Zheng, B. Yan and C. Wu, Water-stable composite of HKUST-1 with its pyrolysis products for enhanced CO_2 capture capacity, *Inorg. Chem. Commun.*, 2022, **146**, 110063.

39 Y. Dong, X. Zhan, X. Niu, J. Li, F. Yuan, Y. Zhu and H. Fu, Facile synthesis of Co-SBA-16 mesoporous molecular sieves

with EISA method and their applications for hydroxylation of benzene, *Microporous Mesoporous Mater.*, 2014, **185**, 97–106.

40 B. B. Pinheiro, S. Saibi, L. Haroune, N. S. Rios, L. R. B. Gonçalves and H. Cabana, Genipin and glutaraldehyde based laccase two-layers immobilization with improved properties: New biocatalysts with high potential for enzymatic removal of trace organic contaminants, *Enzyme Microb. Technol.*, 2023, **169**, 110261.

41 Q. Liu, Y. Wang, X. Liu, S. Li, S. Ren, Z. Gao, T. Han, Z. Xu and H. Zhou, Glutaraldehyde base-cross-linked chitosan-silanol/Fe_3O_4 composite for removal of heavy metals and bacteria, *Environ. Sci. Pollut. Res.*, 2022, **29**, 69439–69449.

42 B. Y. Liu, G. M. Zhang, X. L. Li and H. Chen, Effect of glutaraldehyde fixation on bacterial cells observed by atomic force microscopy, *Scanning*, 2012, **34**, 6–11.

43 L.-X. Jiang, L. Guo, J. P. Shapleigh, Y. Liu, Y. Huang, J.-S. Lian, L. Xie, L.-W. Deng, W.-G. Wang and L. Wang, The long-term effect of glutaraldehyde on the bacterial community in anaerobic ammonium oxidation reactor, *Bioresour. Technol.*, 2023, **385**, 129448.

44 F. Liu, H. Liu, H. Zhu, Y. Xie, D. Zhang, Y. Cheng, J. Zhang, R. Feng and S. Yang, Remediation of petroleum hydrocarbon-contaminated groundwater by biochar-based immobilized bacteria, *Biochem. Eng. J.*, 2023, **197**, 108987.

45 A. H. Jawad, N. S. A. Mubarak and A. S. Abdulhameed, Tunable Schiff's base-cross-linked chitosan composite for the removal of reactive red 120 dye: Adsorption and mechanism study, *Int. J. Biol. Macromol.*, 2020, **142**, 732–741.

46 M. H. To, H. Wang, T. N. Lam, G. Kaur, S. L. K. W. Roelants and C. S. K. Lin, Influence of bioprocess parameters on sophorolipid production from bakery waste oil, *Chem. Eng. J.*, 2022, **429**, 132246.

47 A. Gęsicka, P. Oleskowicz-Popiel and M. Łężyk, Recent trends in methane to bioproduct conversion by methanotrophs, *Biotechnol. Adv.*, 2021, **53**, 107861.

48 S. K. S. Patel, R. K. Gupta, V. C. Kalia and J.-K. Lee, Integrating anaerobic digestion of potato peels to methanol production by methanotrophs immobilized on banana leaves, *Bioresour. Technol.*, 2021, **323**, 124550.

49 R. K. Srivastava, P. K. Sarangi, L. Bhatia, A. K. Singh and K. P. Shadangi, Conversion of methane to methanol: Technologies and future challenges, *Biomass Convers. Biorefin.*, 2022, **12**, 1851–1875.

50 M. Prathaban, R. Prathiviraj, R. Mythili, N. Sharmila Devi, M. Sobanaa, J. Selvin and C. Varadharaju, Integrated bioprocess for carbon dioxide sequestration and methanol production, *Bioresour. Technol.*, 2024, **404**, 130847.